Stabilization of a Magnetically Levitated Rotor in the Case of a Defective Radial Actuator

Markus Hutterer, *Member, IEEE*, Dominik Wimmer, and Manfred Schrödl, *Member, IEEE*

***Abstract*—This article describes an operation mode for the stabilization of a 5-DOF active magnetic bearing system in the case of a damaged radial actuator. The proposed method has the task to stabilize the underactuated rotor to ensure a safe deceleration. The resulting underactuated system is not reachable for the admissible angular velocity range. Thus, the rotor could be destabilized for some operating points. However, for a real system with a nonideal isotropic magnetic behavior, the system is reachable for all angular velocities. For the stabilization of the underactuated system, PID controllers are used. The parameters of the PID controllers are calculated using the linear quadratic regulator method. This simple realization of the controllers implies a short computing time. To show the stability and the robustness of the designed controllers, different root loci are visualized. The proposed operating mode is able to prevent the safety bearings from wear and damage in the case of a defective magnetic actuator. Finally, the underactuated operation mode is experimentally validated on a turbomolecular pump, where the center of gravity is not located between the magnetic actuators.**

***Index Terms*—Active magnetic bearing (AMB), proportional-integral differential (PID), turbomolecular pump (TMP), underactuated.**

I. Introduction

ACTIVE magnetic bearings (AMBs) exhibit several advantages compared to conventional bearing systems, such as almost no friction losses, wearless, the ability of long-term high-speed running, and the possibility to affect the mechanical properties [1], [2]. They do not need lubricants and are maintenance free. Thus, the magnetic levitation technology finds its usage in many fields of applications [3]–[6]. There are two major kinds of AMBs. The first type is the electromagnetic bearing that generates the force totally by electromagnets. The other type is the hybrid magnetic bearing, where permanent magnets are used to generate the bias flux and electromagnets to generate the stabilization forces [7]. AMBs are unstable in an open-loop operation and for a stable levitation, they need a position information of the rotor to close the loop by using a position controller. For the position information, typically sensors are used, but in the last years also, self-sensing strategies were developed, such as the INFORM method, which is described in [8] and [9]. 5-DOF AMB system can be approximated with a linear coupled parameter variant system. Due to the coupling of such a multiple-input and multiple-output (MIMO) system, the controller design with classical methods can induce problems. A few control methods are proposed for many different applications of magnetic bearings in the literature. The most straightforward method is the decentralized control, where every sensor is fed back to the actuator of the same degree of freedom [2]. The disadvantage of this simple method is that it leads to nonzero nondiagonal terms in the input and output matrix in the state-space description, which couple the tilting and the translation movement of the rotor. The decoupled control, which is described in [1], decouples the translation and tilting movement with input and output transformations. Due to the parameter variance of an AMB, system stability cannot be ensured for wide operation ranges of the angular velocity. To solve this problem, a compensation of the parameter variance was developed in [10] and [11]. In [12], a decoupling approach for a flexible body system is given. Stabilization methods with optimal state feedback controllers were developed in [10], [13]–[16]. An AMB is generally a nonlinear system. Due to this nonlinear nature of AMBs, the use of Linear Time Invariant (LTI) controllers could lead to problems. The works in [7] and [17] solved this problem using a nonlinear feedback linearization based on differential geometric methods. Other nonlinear approaches are explained in [18]–[21].

In contrast to state-of-the-art control structures, the aim of this article is the stabilization of the rotor in the case of a nonfunctional actuator by switching from the standard operation to a fault operation mode. The fault operation mode is a very important feature to increase the lifecycle of the touch down bearings and, therefore, the maintenance interval of AMB systems. For an actuator failure, the magnetic bearing system is not fully actuated anymore and becomes underactuated. Hence, the control system has the task to calculate the currents of one radial bearing dependent on the position information of four position sensors. Control methods for stabilizing underactuated systems are already described in many publications in the field of robotics [22]–[25]. A related underactuated problem is the inverted pendulum where control methods are described in [26] and [27]. The biggest difference between the inverted pendulum and the underactuated magnetic bearing lies in the remaining negative stiffness of the defective actuator. Thus, the focus of

Manuscript received February 18, 2019; revised August 19, 2019 and February 17, 2020; accepted March 24, 2020. Date of publication April 6, 2020; date of current version December 14, 2020. Recommended by Technical Editor M. Indri. *(Corresponding author: Markus Hutterer.)*

The authors are with the Institute of Energy Systems and Electrical Drives, Vienna University of Technology, 1040 Vienna, Austria (e-mail: markus.hutterer@tuwien.ac.at; dominik.wimmer@tuwien.ac.at; manfred.schroedl@tuwien.ac.at).

Color versions of one or more of the figures in this article are available online at http://ieeexplore.ieee.org.

Digital Object Identifier 10.1109/TMECH.2020.2985623

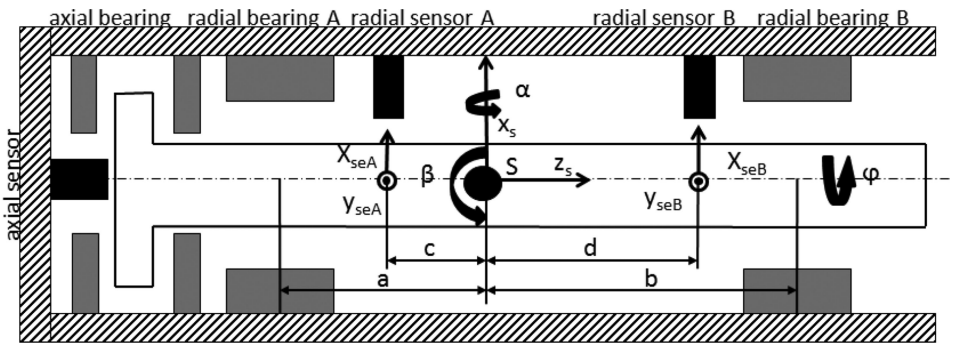

Fig. 1. 5-DOF AMB system.

this article lies in the development and experimental validation of the underactuated magnetic bearing system in the case of a defective actuator. Such an actuator failure can be detected by measuring and evaluating the actuator currents.

In [28]–[31], fault-tolerant magnetic bearings are developed.

In contrast to the development of fault-tolerant bearings, the proposed structure has the following characteristics.

(1) The proposed structure can also be used if the control part of one radial bearing fails completely.
(2) The topology of the bearings is not important for the proposed control structure, because the mechanical coupling between both bearings is used for stabilization.

Based on Tedrake [32], an underactuated system with the degrees of freedom $\mathbf{q}$ of an affine mechanical system

$$\ddot{\mathbf{q}} = \mathbf{f}_1(\mathbf{q}, \dot{\mathbf{q}}, t) + \mathbf{f}_2(\mathbf{q}, \dot{\mathbf{q}}, t)\,\mathbf{u} \tag{1}$$

is defined as follows:

Definition 1: A control system described by (1) is fully actuated in configuration $(\mathbf{q}, \dot{\mathbf{q}}, t)$ if it is able to command an instantaneous acceleration in an arbitrary direction in $\mathbf{q}$

$$\operatorname{rank}\left[\mathbf{f}_2(\mathbf{q}, \dot{\mathbf{q}}, t)\right] = \dim\left[\mathbf{q}\right]. \tag{2}$$

Definition 2: A control system described by (1) is underactuated in configuration $(\mathbf{q}, \dot{\mathbf{q}}, t)$ if it is not able to command an instantaneous acceleration in an arbitrary direction in $\mathbf{q}$

$$\operatorname{rank}\left[\mathbf{f}_2(\mathbf{q}, \dot{\mathbf{q}}, t)\right] < \dim\left[\mathbf{q}\right]. \tag{3}$$

The proposed operation mode should be able to stabilize the rotor in the case of an actuator failure by switching from a fully actuated operation mode to an underactuated operation mode. However, the rank deficiency of the input matrix $\mathbf{f}_2(\mathbf{q}, \dot{\mathbf{q}}, t)$ caused by the underactuation does not imply that it is not possible to reach every position. In fact, if the reachability matrix of the underactuated system has full rank, it is possible to reach every state from any initial condition at some time t_1 (although the reached state may not be an equilibrium). In order to get a low computing time of the resulting control structure, the system is assumed to behave linear.

II. 5-DOF AMB System

A rigid body has three tilting (α, β, φ) and three translation (x_s, y_s, z_s) degrees of freedom. The stabilization of the 5-DOF rigid rotor requires constraints, which are provided by magnetic actuators. A common magnetic bearing system consists of two radial bearings and one axial bearing. Fig. 1 shows an illustration of a 5-DOF AMB system. The only degree of freedom that is not controlled by magnetic bearings is angle φ. To achieve a stable levitation, each degree of freedom has to be observable. For observation, the common-type AMB system has five position sensors to close the control loop. If the AMB system is detectable and stabilizable, it is possible to design a control structure that can stabilize the rotor. Compared to fully observability and fully reachability, these are weaker conditions, because reachability and observability are only required for the unstable poles.

For a model-based controller design, the system equation has to be derived. In this article, the radial and axial bearings are separated for the controller design. This is possible under a few assumptions, which are described in [1]. Thus, only the radial behavior is investigated in this publication.

The equation of motion of a rigid rotor using Newton's equations for the translation movements and Euler's equations for the tilting movements has the following form for the radial movement:

$$\mathbf{M}\ddot{\mathbf{x}} + \mathbf{G}(\Omega)\dot{\mathbf{x}} = \mathbf{f} \tag{4}$$

with

$$\mathbf{M} = \begin{bmatrix} I_e & 0 & 0 & 0 \\ 0 & m & 0 & 0 \\ 0 & 0 & I_e & 0 \\ 0 & 0 & 0 & m \end{bmatrix} \qquad \mathbf{x} = \begin{bmatrix} \beta \\ x_s \\ \alpha \\ y_s \end{bmatrix}$$

$$\mathbf{G}(\Omega) = \begin{bmatrix} 0 & 0 & I_p\Omega & 0 \\ 0 & 0 & 0 & 0 \\ -I_p\Omega & 0 & 0 & 0 \\ 0 & 0 & 0 & 0 \end{bmatrix} \qquad \mathbf{f} = \begin{bmatrix} M_\beta \\ f_{Sx} \\ M_\alpha \\ f_{Sy} \end{bmatrix} \tag{5}$$

where m and I_e define the mass and the equatorial moment of inertia, respectively, I_p is the polar moment of inertia, the components of the vector $\mathbf{x}$ are the degrees of freedom of the center of gravity (COG) coordinate system, and the components of the vector $\mathbf{f}$ are the forces and torques in the COG system.

Equation (4) is subjected to the following assumptions [1].

1) The rotor is rotational symmetric and rigid.

2) Deviations from the reference position are small compared to the rotor dimensions.
3) The angular velocity $\Omega = \dot{\varphi}$ is assumed to be constant or slowly changing in contrast to the system dynamics.

The force vector $\mathbf{f}$ is provided by magnetic bearings, which underlies the following linearized equation:

$$\mathbf{f} = \mathbf{B}\mathbf{K}_x\mathbf{B}^T\mathbf{x} + \mathbf{B}\mathbf{K}_i\mathbf{i} \tag{6}$$

with

$$\mathbf{B} = \begin{bmatrix} a & b & 0 & 0 \\ 1 & 1 & 0 & 0 \\ 0 & 0 & a & b \\ 0 & 0 & 1 & 1 \end{bmatrix} \quad \mathbf{K}_i = \begin{bmatrix} k_{iA} & 0 & 0 & 0 \\ 0 & k_{iB} & 0 & 0 \\ 0 & 0 & k_{iA} & 0 \\ 0 & 0 & 0 & k_{iB} \end{bmatrix} \tag{7}$$

$$\mathbf{K}_x = \begin{bmatrix} k_{xA} & 0 & 0 & 0 \\ 0 & k_{xB} & 0 & 0 \\ 0 & 0 & k_{xA} & 0 \\ 0 & 0 & 0 & k_{xB} \end{bmatrix} \mathbf{i} = \begin{bmatrix} i_{xA} \\ i_{xB} \\ i_{yA} \\ i_{yB} \end{bmatrix}. \tag{8}$$

$\mathbf{B}$ is the input matrix, which transforms the forces of the actuator in the COG coordinate system. The components of $\mathbf{K}_x$ and $\mathbf{K}_i$ are the force displacement (negative stiffness) and the force current factors, which result from linearization of the force generation of the magnetic actuators. Both matrices have a diagonal form. Combining (4) with (6) and extending it with the output equation leads to the linearized system equation of the radial AMB system

$$\begin{aligned} \mathbf{M}\ddot{\mathbf{x}} + \mathbf{G}(\Omega)\dot{\mathbf{x}} - \mathbf{B}\mathbf{K}_x\mathbf{B}^T\mathbf{x} &= \mathbf{B}\mathbf{K}_i\mathbf{i} \\ \mathbf{y} &= \mathbf{C}\mathbf{x} \end{aligned} \tag{9}$$

with

$$\mathbf{C} = \begin{bmatrix} c & 1 & 0 & 0 \\ d & 1 & 0 & 0 \\ 0 & 0 & c & 1 \\ 0 & 0 & d & 1 \end{bmatrix} \mathbf{y} = \begin{bmatrix} x_{seA} \\ x_{seB} \\ y_{seA} \\ y_{seB} \end{bmatrix} \tag{10}$$

where $\mathbf{C}$ is the output matrix, which transforms the COG coordinates to the sensor coordinates and the components of $\mathbf{y}$ define the positions measured by the sensors. The system equation (9) describes a mechanical system with a coupled negative stiffness $\mathbf{B}\mathbf{K}_x\mathbf{B}^T$ and a parameter variant matrix $\mathbf{G}(\Omega)$. If all actuators are operating, the system fulfills the requirement from (2). Thus, a decoupling approach can be used for the controller design. In the case of a defective radial actuator, the system becomes underactuated according to Definition 2. In this case, the couplings of the system are required for a stabilization of the rotor.

III. Control Structure for the Fully Actuated System

This section should give an overview of the control structure for the fully actuated system, which has already been explained in detail in [11]. An illustration of the control structure is shown in Fig. 2. As stated in the previous section, the controller for the fully actuated system is based on a decoupling approach. Therefore, an input transformation matrix $\mathbf{T}_{\text{in}}$ and an output transformation matrix $\mathbf{T}_{\text{out}}$ are introduced. With

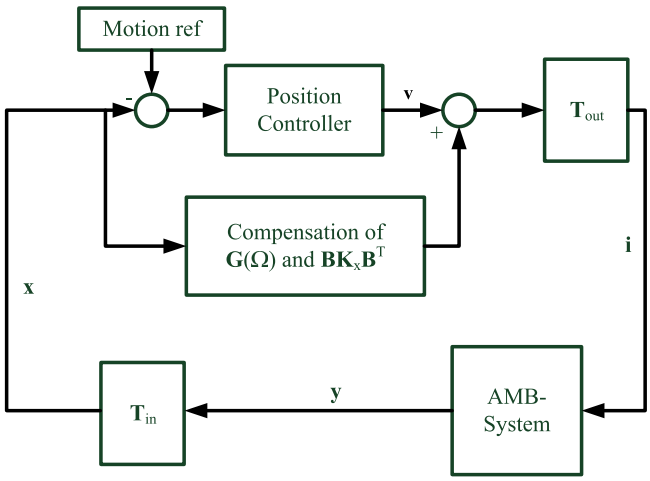

Fig. 2. Control structure of the fully actuated system.

$$\mathbf{T}_{\text{in}} = \mathbf{C}^{-1} \qquad \mathbf{T}_{\text{out}} = (\mathbf{B}\mathbf{K}_i)^{-1} \tag{11}$$

the sensor coordinates are transformed to the COG coordinates and the system equation has the following form:

$$\mathbf{M}\ddot{\mathbf{x}} + \mathbf{G}(\Omega)\dot{\mathbf{x}} - \mathbf{B}\mathbf{K}_x\mathbf{B}^T\mathbf{x} = \mathbf{i}_{\text{COG}}. \tag{12}$$

Because the mass matrix $\mathbf{M}$ has a diagonal form, it is not necessary to cancel this term. The implemented controller law for the fully actuated system is

$$\mathbf{i}_{\text{COG}} = \mathbf{v} - \mathbf{B}\mathbf{K}_x\mathbf{B}^T\mathbf{T}_{\text{in}}\mathbf{y} + \mathbf{G}(\Omega)\dot{\mathbf{x}} \tag{13}$$

with

$$\mathbf{v} = -\mathbf{T}_{\text{con}}\mathbf{T}_{\text{in}}\mathbf{y} \tag{14}$$

where $\mathbf{T}_{\text{con}}$ defines the transfer function matrix of the applied position controller. With this control structure, the system has the following decoupled form:

$$\mathbf{M}\ddot{\mathbf{x}} = \mathbf{v}. \tag{15}$$

The position controller has the task to stabilize the decoupled system and the bending modes. This is done by using PID controllers in combination with second-order filters to shift the phase for providing damping in the range of the bending modes [10], [11], [33], [34].

IV. Underactuated System for a Defective Radial Actuator at Standstill

The aim of this section is to derive a control law, which is able to stabilize the rotor in the case of an actuator failure. Before the control structure for the complete magnetic bearing is explained, some basic ideas will be discussed for a two-dimensional simplification of the system. However, this simplification can always be used for standstill.

For deriving the control law, the axial movement is assumed to be decoupled from the radial movement. Therefore, the axial

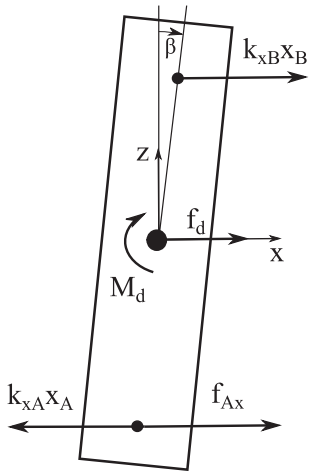

Fig. 3. Forces on the rotor of the underactuated system for an defective actuator B in the *xz* plane.

movement is not considered in this article, because the design procedure is well known from the literature. Fig. 3 shows the forces in the case of a breakdown of the actuator B. Only the impact of the negative stiffness is left at the damaged actuator. This is the case with hybrid magnetic bearings or with AMBs where only the supply of the bias current works. The equation of motion for the underactuated system follows from (9) by the elimination of one actuator (e.g., actuator B)

$$\mathbf{M}_x\ddot{\mathbf{x}}_x - \mathbf{B}_x\mathbf{K}_{xx}\mathbf{B}_x^T\mathbf{x}_x = \mathbf{B}_{\mathrm{ua}x}k_{iA}i_A + \mathbf{f}_d \quad \mathbf{f}_d = \begin{bmatrix} M_d \\ f_d \end{bmatrix} \tag{16}$$

where the identifier x defines the matrices of the movement in the *xz* plane, $\mathbf{B}_{\mathrm{ua}x}$ describes the input matrix of the underactuated system, and $\mathbf{f}_d$ describes the impact of possible constant disturbance forces or torques. Using (3), the system of (16) can be classified as an underactuated system. For such a system, a decoupled control strategy is not possible, because the system has more outputs than inputs. The possibility of stabilization depends on the stabilizability and the detectability of the system. For the first analysis, the disturbance forces $\mathbf{f}_d$ are neglected. To test the stabilizability and the detectability, the system is transformed in a state- space representation

$$\begin{aligned} \dot{\mathbf{z}} &= \mathbf{A}\,\mathbf{z} + \mathbf{B}_{s,\mathrm{ua}x}\,i_A \\ \mathbf{y} &= \mathbf{C}_s\,\mathbf{z}. \end{aligned} \tag{17}$$

The determinant of the reachability matrix of the underactuated system is

$$\det(\mathcal{R}\,(\mathbf{A}, \mathbf{B}_{s,\mathrm{ua}x})) = -\frac{k_{iA}^4 k_{xB}^2 (a-b)^2 (a\,b\,m + I_e)^2}{I_e^4 m^4}. \tag{18}$$

The system is not reachable if this determinant is zero. Solving the equation

$$\det(\mathcal{R}\,(\mathbf{A}, \mathbf{B}_{s,\mathrm{ua}x})) = 0 \tag{19}$$

under the conditions $k_{xB} \neq 0$ and $k_{iA} \neq 0$ leads to the following conditions where the system is not reachable:

$$a = b \qquad a = -\frac{I_e}{b\,m}. \tag{20}$$

The first condition is not from practical interest and describes a system where both actuators act on the same place of the rotor. To explain the physical reason of the second condition, the matrix of the eigenvectors $\mathbf{V} = [\mathbf{x}_{e,1}, \mathbf{x}_{e,2}]$ of the eigenvalue problem

$$-(\mathbf{B}_x\mathbf{K}_{xx}\mathbf{B}_x^T)^{-1}\mathbf{M}\,\mathbf{x}_{e,i} = \lambda\mathbf{x}_{e,i} \tag{21}$$

for condition (20) is calculated

$$\mathbf{V} = \begin{bmatrix} \frac{b\,m}{I_e} & -\frac{1}{b} \\ 1 & 1 \end{bmatrix}. \tag{22}$$

For calculating the nodes, the zero crossing of the mode shapes is calculated

$$z_{0,1} = -\frac{I_e}{b\,m} = a \quad z_{0,2} = b. \tag{23}$$

Thus, the physical reason of the uncontrollable behavior are that the nodes of the mode shapes lies at the points of actuation. If the conditions (20) and $c = d$ are not true, the system is reachable and observable. The condition $c = d$ for the observability of the system can be derived in a similar way as the reachability. With that knowledge, the observability and reachability can also be calculated for the three-dimensional underactuated system at standstill, because there is no coupling between the *xz* and *yz* plane at standstill.

An important difference compared to the fully actuated system is that it is not possible to reach every steady-state position. From the equilibrium of the torques and forces

$$\begin{aligned} \Sigma f_x = 0 = \quad & k_{xB}x_B - k_{xA}x_A + f_{Ax} \\ \Sigma M^{(A)} = 0 = \quad & -k_{xB}x_B(b-a) \end{aligned} \tag{24}$$

can be calculated that the system has to fulfill the constraint $x_B = 0$ at steady state for $\mathbf{f}_d = \mathbf{0}$.

In real applications, constant disturbance forces $\mathbf{f}_d \neq \mathbf{0}$ are always present. In the application field of magnetic bearings, these disturbance forces can be caused, for example, by a non-colocation of the geometric center and the magnetic center or by the gravity. Someone might think that it is impossible to stabilize the rotor in the presence of disturbance forces, because the force f_{Ax} cannot compensate the translation and the rotation part of $\mathbf{f}_d$. This is only true if the AMB bias flux is zero. In the case of a permanent magnet biased AMB or if only the control part of actuator B is defect, the negative stiffness could be used to stabilize the system. In contrast to the system without disturbance forces, the steady state has to fulfill the constraint

$$x_B = \frac{M_d - a\,f_d}{k_{xB}(a-b)} \tag{25}$$

which depends on the entries of $\mathbf{f}_d$, the position of the actuators, and the negative stiffness k_{xB}. Equation (25) shows that it is impossible to reach the center position at standstill. To get close to the center position, the negative stiffness could be increased. However, a high negative stiffness will also increase the required

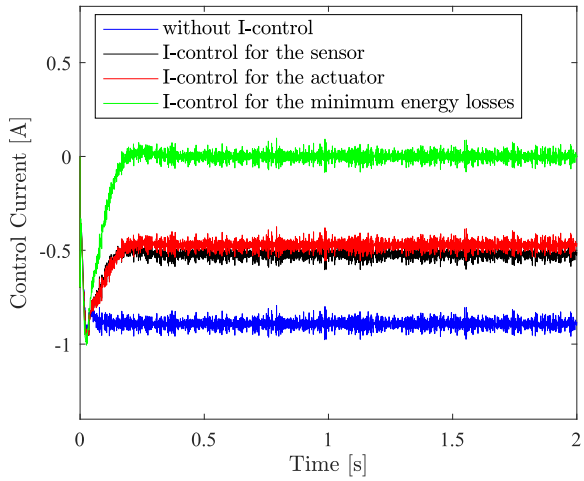

Fig. 4. Control current for different stationary states at the working actuator for the underactuated operation.

bandwidth and the sensitivity of the system. It also has to be considered that the negative stiffness could only be treated as linear near the center position.

For the fully actuated system, the integration action of the position controller should keep the rotor in the center position. For the underactuated system, this is not possible, because of the constraint (25). The stationary point of the working actuator x_A could be chosen with the aim to optimize the usage of the mechanical air gap. Another impact of this choice lies in the current consumption, as can be seen in Fig. 4, where four different cases were evaluated. For the constant disturbance, the gravity force was chosen. The blue line is only a stabilizing controller without an integration action. The red and black lines show the current consumption with an integration action to eliminate the stationary failure at the actuator A or at the sensor A. The green line shows the optimized steady state for minimizing the current consumption. This optimized steady state can be reached if the motion reference signal of the integration action is the same as the equilibrium position of the rotor for zero current. It has to be mentioned that the system with constant disturbance forces can only be used, if the mechanical gap allows the constraint (25). For many magnetic bearing systems, this fact limits the usage of the proposed control method for horizontal operation.

V. Underactuated Rotating System

For the rotating system only, one radial magnetic bearing can be controlled. The second magnetic bearing (e.g., bearing A) is constantly premagnetized by electrical currents or permanent magnets. The equation of motion of the underactuated three-dimensional system is

$$\mathbf{M}\ddot{\mathbf{x}} + \mathbf{G}(\Omega)\dot{\mathbf{x}} - \mathbf{B}\mathbf{K}_x\mathbf{B}^T\mathbf{x} = \mathbf{B}_{\text{ua}}\mathbf{K}_{i\text{ua}}\mathbf{i}_{\text{ua}} \tag{26}$$

with

$$\mathbf{B}_{\text{ua}} = \begin{bmatrix} b & 0 \\ 1 & 0 \\ 0 & b \\ 0 & 1 \end{bmatrix} \quad \mathbf{K}_{i\text{ua}} = \begin{bmatrix} k_{iB} & 0 \\ 0 & k_{iB} \end{bmatrix} \quad \mathbf{i}_{\text{ua}} = \begin{bmatrix} i_{xB} \\ i_{yB} \end{bmatrix}. \tag{27}$$

In contrast to the two-dimensional case, the system is parameter-variant due to the gyroscopic effect. The gyroscopic effect splits up the eigenvalues of the tilting movement in a nutation and a precession mode. The natural frequency of the nutation mode increases with increasing angular velocity and the precession mode decreases. Thus, the nutation mode gives a lower limit on the bandwidth of the system. The parameter variance caused by the gyroscopic effect changes the reachability for different angular velocities.

The system is not reachable if the reachability matrix $\mathcal{R}(\mathbf{A}_{rot}, \mathbf{B}_{s,\text{ua}})$ has a lower rank as the number of state variables. The matrices $\mathbf{A}_{rot}$ and $\mathbf{B}_{s,\text{ua}}$ describes the dynamic and the input matrix of the rotating underactuated system in the state-space representation with the state vector $\mathbf{z}_r = [\mathbf{x}\ \dot{\mathbf{x}}]^T$. In contrast to the two-dimensional system, the reachability matrix is not quadratic for the rotating systems. Thus, the circumstance is used that the rank of a matrix is given by the number of the nonzero singular values. Therefore, the matrix $\mathcal{R}(\mathbf{A}_{rot}, \mathbf{B}_{s,\text{ua}})$ has not the full rank and the system is not reachable for the following condition:

$$\det(\mathcal{R}\left(\mathbf{A}_{rot}, \mathbf{B}_{s,\text{ua}}\right)\mathcal{R}\left(\mathbf{A}_{rot}, \mathbf{B}_{s,\text{ua}}\right)^T) = 0. \tag{28}$$

Solving (28) leads to

$$\Omega_{uc} = \pm\frac{(I_e + b\,m\,a)\sqrt{b\,k_{xA}\,m\,(a-b)}}{I_p\,b\,m}. \tag{29}$$

From (29), it can be concluded that the system is not reachable for a defined speed if the COG is on the right-hand side of actuator B ($a < 0$, $b < 0$, and $a < b$) according to Fig. 1. If the COG lies between the actuators ($a < 0$ and $b > 0$) or the COG lies on the left-hand side of actuator A ($a > 0$, $b > 0$, and $a < b$), (29) would result in an imaginary angular velocity. Also, condition (20) is present in (29) if Ω_{uc} is set to zero.

Equation (29) only shows that an angular velocity exists where the system is not reachable. However, this condition is not enough to know if the system can be stabilized for the considered angular velocities Ω_{uc}. If the underactuated AMB can be stabilized or not depends on the stability of the not reachable subsystem. To calculate the not reachable subsystem, a state transformation $\mathbf{z}_r = \mathbf{V}\tilde{\mathbf{z}}_r$ is introduced with the state vector of the rotating system $\mathbf{z}_r$ and the transformation matrix

$$\mathbf{V} = \begin{bmatrix} \mathbf{B}_{s,\text{ua}} & \mathbf{A}_{rot}\mathbf{B}_{s,\text{ua}} & \mathbf{A}_{rot}^2\mathbf{B}_{s,\text{ua}} & \mathbf{K} \end{bmatrix} = \begin{bmatrix} \mathbf{H} & \mathbf{K} \end{bmatrix} \tag{30}$$

where $\mathbf{H}$ is the first part of $\mathcal{R}(\mathbf{A}_{rot}, \mathbf{B}_{s,\text{ua}})$ until the rank is equal to the rank $\mathcal{R}(\mathbf{A}_{rot}, \mathbf{B}_{s,\text{ua}})$ and $\mathbf{K}$ consist of linear independent vectors in a way that the rank of $\mathbf{V}$ is equal to the number of states. The matrix $\mathbf{K}$ can be chosen with

$$\mathbf{K} = \begin{bmatrix} 0 & 0 & 0 & 0 & 0 & 0 & 1 & 0 \\ 0 & 0 & 0 & 0 & 1 & 0 & 0 & 0 \end{bmatrix}^T \tag{31}$$

and the transformed system can be given as

$$\begin{bmatrix} \dot{\tilde{\mathbf{z}}}_{r,1} \\ \dot{\tilde{\mathbf{z}}}_{r,2} \end{bmatrix} = \begin{bmatrix} \mathbf{A}_{11} & \mathbf{A}_{12} \\ \mathbf{0} & \mathbf{A}_{22} \end{bmatrix} \begin{bmatrix} \tilde{\mathbf{z}}_{r,1} \\ \tilde{\mathbf{z}}_{r,2} \end{bmatrix} + \begin{bmatrix} \mathbf{B}_1 \\ \mathbf{0} \end{bmatrix} \mathbf{i}_{\text{ua}} \tag{32}$$

with the dynamic matrix of the not reachable subsystem

$$\mathbf{A}_{22} = \begin{bmatrix} 0 & \dfrac{k_{xA}\,(a-b)}{\sqrt{b\,m\,k_{xA}\,(a-b)}} \\ -\dfrac{k_{xA}\,(a-b)}{\sqrt{b\,m\,k_{xA}\,(a-b)}} & 0 \end{bmatrix}. \quad (33)$$

The eigenvalues of the not reachable dynamic matrix $\mathbf{A}_{22}$ are

$$\lambda_{1,2} = \pm\frac{\sqrt{-b\,m\,k_{xA}(a-b)}}{b\,m}. \quad (34)$$

As stated from (29), the system is not reachable for a specified angular velocity if the COG lies on the right-hand side of actuator B ($b < 0$). Thus, (34) is only valid for the not reachable case. Under the condition $b < 0$, the not reachable subsystem is marginally stable from the theoretical point of view.

The physical reason for the loss of reachability lies in speed-depended mode shapes caused by the gyroscopic effect. For obtaining the mode shape of the not reachable subsystem, the eigenvectors ($\mathbf{x}_r$, $\bar{\mathbf{x}}_r$) for the eigenvalues (34) are calculated. $\bar{\mathbf{x}}_r$ defines the conjugate complex value of $\mathbf{x}_r$. The first n elements of the eigenvectors $\mathbf{x}_r$

$$\begin{bmatrix}\mathbf{x}_r(1) & \dots & \mathbf{x}_r(4)\end{bmatrix}^T = \begin{bmatrix}1 & -b & j & -j\,b\end{bmatrix}^T \quad (35)$$

correspond to the modes of the system [35], where n is the number of the degrees of freedom. Thus, the node of the mode shape (35) is at the same place as the actuator B, and therefore, the current vector $\mathbf{i}_{ua}$ has no impact on the unreachable dynamic (33).

However, real systems always have some damping due to air friction or other physical reasons. Also, the simulated ideal isotropic behavior of the magnetic bearings ($k_{x,x}$=$k_{x,y}$) cannot be fulfilled exactly for real systems.

By using (28), for bearings with an anisotropic behavior, it can be shown that the system is reachable if condition (20) is not fulfilled.

VI. Controller Design

The mechanical model of the magnetic bearing system is described by a MIMO parameter-variant system caused by the gyroscopic effect. The control structure of the underactuated system is illustrated in Fig. 5.

The transfer matrix of the controller is given by

$$\mathbf{PID}(s) = \begin{bmatrix} C_{11} & C_{12} & C_{13} & C_{14} \\ C_{21} & C_{22} & C_{23} & C_{24} \end{bmatrix}. \quad (36)$$

The cross-couplings of the translation coordinates x_S and y_S are small in many cases. Thus, the related couplings C_{14} and C_{22} can often be neglected.

The angular velocity Ω can be interpreted as a variant parameter of the magnetic bearing equation. Thus, for a constant Ω, optimal control algorithms, such as H_∞ or linear quadratic regulator (LQR), can be applied. To overcome the parameter variance, the controller transfer matrix is gain scheduled. The step size of gain scheduling has to be low enough to provide robust and well-performed controllers in the operating ranges.

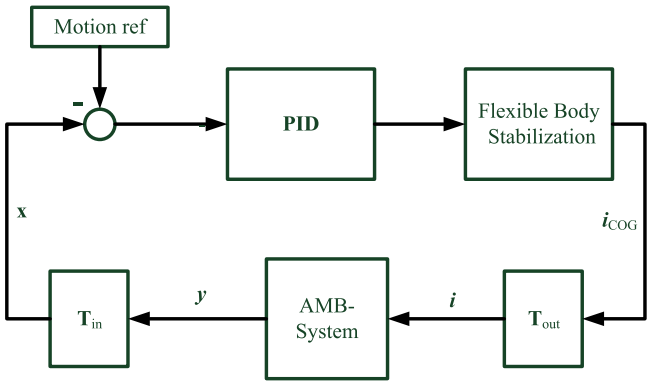

Fig. 5. Control structure of the underactuated system.

However, a too small step size can cause too much switching actions in a defined time range. The main advantage of the LQR is the direct relation of the weighting matrices to the manipulated variables and the dynamic of the states. The main drawback is that the eigenvalues cannot be specified. Therefore, the eigenvalues of the rigid body model can influence the bending modes and cause an unstable system. Hence, the rigid-body eigenvalues have to provide a high enough separating margin to the flexible body modes.

A. Controller Design Using the LQR Method

In a first step, an LQR is designed using the assumption that all states are measurable. Compared to other controller design techniques, the LQR seeks to find an optimum that minimizes a cost function

$$J(x_0) = \sum_{k=0}^{N-1} \left(\mathbf{z}_k^T\mathbf{Q}\mathbf{z}_k + \mathbf{u}_k^T\mathbf{R}\mathbf{u}_k + 2\mathbf{u}_k^T\mathbf{N}\mathbf{z}_k\right) \quad (37)$$

for the discretized magnetic bearing system

$$\begin{aligned}\mathbf{z}_{k+1} &= \mathbf{\Phi}\mathbf{z}_k + \mathbf{\Gamma}\mathbf{u}_k \\ \mathbf{y}_k &= \mathbf{C}\mathbf{z}_k.\end{aligned} \quad (38)$$

The calculated LQR parameters can be used directly in PID controllers in a next step. In real magnetic bearing, systems always constant disturbances occur, e.g., the gravity force or a noncollocation, between the geometric center and the magnetic center. To eliminate the constant disturbances, the system is extended with an integration state for optimization

$$\mathbf{z}_{I,k+1} = \mathbf{z}_{I,k} + (\mathbf{r}_k - \mathbf{C}_2\mathbf{z}_k) \quad (39)$$

where $\mathbf{r}_k$ is the reference signal and $\mathbf{C}_2$ is a 2×8 matrix, which defines the input of the integration parts [because of condition (25) it is not possible to satisfy the requirements of four independent integration parts]. An extension of the discrete system equation (38) with the integration states (39) yields

$$\begin{bmatrix}\mathbf{z}_{k+1} \\ \mathbf{z}_{I,k+1}\end{bmatrix} = \begin{bmatrix}\mathbf{\Phi} & \mathbf{0} \\ -\mathbf{C}_2 & \mathbf{I}\end{bmatrix}\begin{bmatrix}\mathbf{z}_k \\ \mathbf{z}_{I,k}\end{bmatrix} + \begin{bmatrix}\mathbf{\Gamma} \\ \mathbf{0}\end{bmatrix}\mathbf{u}_k + \begin{bmatrix}\mathbf{0} \\ \mathbf{I}\end{bmatrix}\mathbf{r}_k \quad (40)$$

where $\mathbf{I}$ is the identity matrix.

TABLE I
PARAMETERS OF THE MAGNETIC BEARING SYSTEM

I_p	0.008780 kg m^2
I_e	0.023900 kg m^2
m	4.5 kg
k_{iA}	26 N/A
k_{iB}	50 N/A
k_{xA}	30.500 N/m
k_{xB}	67.000 N/m
b	−0.02 m
a	−0.099 m
c	−0.119 m
d	0.0024 m

According to Ahrens *et al.* [36], an LQR has a low stability margin for high rotational speeds. To increase the stability margin, the system equation for the optimization process is changed as follows:

$$\mathbf{z}_{k+1} = \tilde{\mathbf{\Phi}}\mathbf{z}_k + \tilde{\mathbf{\Gamma}}\mathbf{u}_k \tag{41}$$

with

$$\tilde{\mathbf{\Phi}} = \frac{1}{r}\mathbf{\Phi} \quad \tilde{\mathbf{\Gamma}} = \frac{1}{r}\mathbf{\Gamma}. \tag{42}$$

Therefore, the poles of the system must lie inside a circle with the radius $r \leq 1$. For the controller design, $\mathbf{N}$ is set to zero. By using higher entries of the matrix $\mathbf{Q}$, the settling times of the states are decreased. Increasing the entries of the matrix $\mathbf{R}$ decrease the required manipulated variables. Therefore, a tradeoff between a suitable settling time and the maximum amplitude of the manipulated variables has to be found.

Solving the LQR optimization problem (37) leads to a constant stabilization matrix $\mathbf{K}_r$ of a state-space controller

$$\mathbf{u}_k = \mathbf{K}_r \begin{bmatrix} \mathbf{z}_k \\ \mathbf{z}_{I,k} \end{bmatrix}. \tag{43}$$

The coefficients of the matrix $\mathbf{K}_r$ have the following relation to the coefficients of the PID controller:

$$\mathbf{K}_r = \begin{bmatrix} P_{11}...P_{14} & D_{11}...D_{14} & I_{11}...I_{12} \\ P_{21}...P_{24} & D_{21}...D_{24} & I_{21}...I_{22} \end{bmatrix} \tag{44}$$

with the proportional parts of the related PID controllers P_{ii}, the related differentiating parts D_{ii} and the related integrating parts I_{ii}.

B. Stability of the Closed-Loop System

For the investigation of the stability, the system parameters of Table I are applied and for the optimization problem, the weighting matrices are chosen with

$$\mathbf{Q} = \text{diag}([1000\ 1000\ 1000\ 1000\ 1\ 1\ 1\ 1])$$
$$\mathbf{R} = \text{diag}([0.1\ 0.1]) \quad r = 1 \quad T_s = 100\,\mu\text{s} \tag{45}$$

with the sampling time T_s. For the sampling, a zero-order hold is modeled.

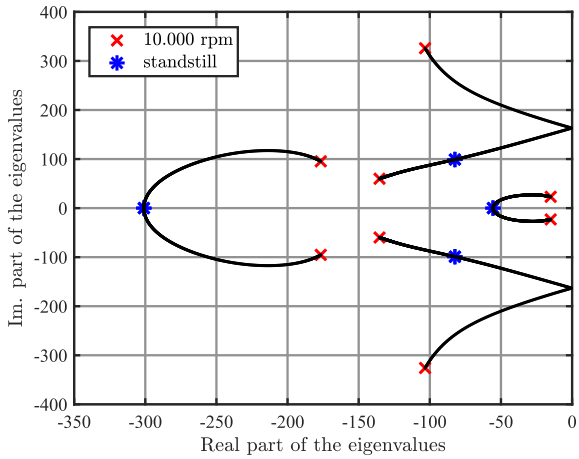

Fig. 6. Root locus of an isotropic underactuated system using a gain scheduled LQR (COG lies on the right-hand side of actuator B).

The eigenvalues of the dynamic matrix of the controlled system

$$\mathbf{A}_c = \mathbf{A}_{rot} - \mathbf{B}_{s,\text{ua}}\,\mathbf{K}_r \tag{46}$$

for different speeds can be visualized using root loci.

For the sake of clarity, the integration parts of the controller are not considered in the root loci. If r is set to a value lower than 1, numerical problems occur by the calculation of the root loci around the marginally stable points. However, for the experimental results, the value for r is changed slightly.

Fig. 6 shows the root locus of a gain scheduled LQR from standstill to an angular velocity of 10.000 r/min for an underactuated AMB system with an isotropic behavior of the magnetic bearings. The blue asterisk signs indicate the eigenvalues at standstill and the red cross for 10.000 r/min. The root locus plot illustrates the absence of reachability for a certain speed range, where one of the conjugate complex pole pairs drift to the imaginary axis. The eigen frequency of the pole pair with zero damping has the same value as the eigen frequency ($\lambda_{1,2} = \pm j163.62$ rad/s) given by (34) for the parameters of Table I. Hence, the loss of damping is caused by the absence of reachability. However, for higher speeds, the damping increases again. All other poles show a suitable damping for the plotted speed range.

In general, it is impossible to design an absolute isotropic AMB system. To illustrate the performance of the AMB system with an anisotropic behavior, the negative stiffnesses are chosen 20 % higher in the x-direction than in the y-direction. Fig. 7 shows that the system is stable in the simulated speed range with an anisotropic behavior. Thus, an underactuated system can be stabilized in many cases by changing the bias flux in the x-direction or in the y-direction.

If the COG lies between the actuators A and B, the reachability of the system is always given if condition (20) is not fulfilled. Therefore, the root locus has a suitable damping in the defined speed range (see Fig. 8). For calculation of the root locus, the same system parameters are used, but only the sign of b was changed.

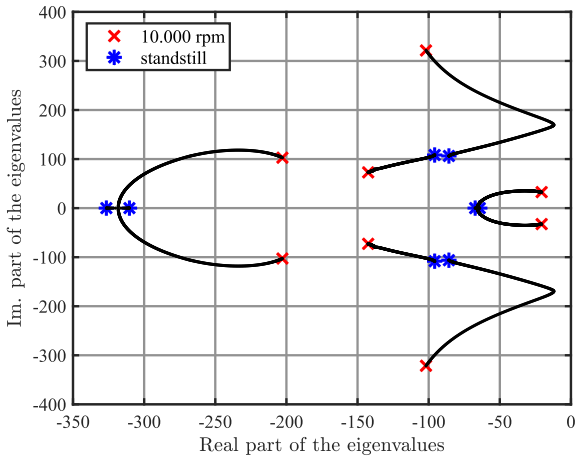

Fig. 7. Root locus of an anisotropic underactuated system using a gain scheduled LQR (COG lies on the right-hand side of actuator B).

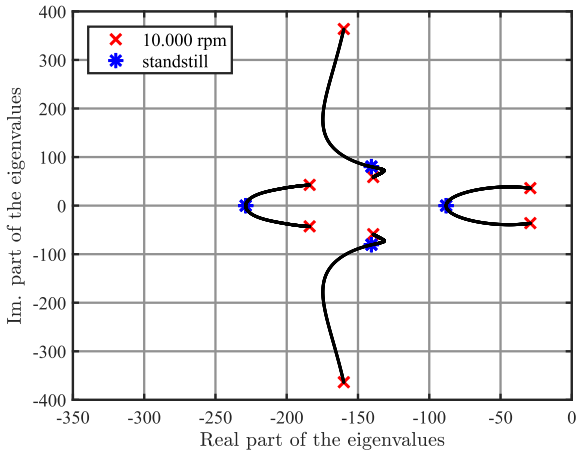

Fig. 8. Root locus of an isotropic underactuated system using a gain scheduled LQR (COG lies between actuators A and B).

VII. Experimental Results

In this section, the performance of the proposed controller is evaluated on a turbomolecular pump (TMP). The control system was implemented on a digital signal processor (TMS320F28335) of a state-of-the-art hardware for magnetic bearings. A schematic illustration of the stabilized rotor can be seen in Fig. 9. The blade wheel illustrates a more complex structure, which is modeled as a rigid part in the simulations. For the position measurement, inductive sensors were used. The actuators are heteropolar AMBs using the "differential driving mode" for operation.

Fig. 10 shows a schematic illustration of the experimental setup. The software MATLAB is used on a personal computer to communicate with the magnetic bearing and the motor controller. The TMP does not need an angle sensor for the motor controller, because the INFORM method [37] is used for controlling the electrical machine.

For the following experiments, the actuator A is assumed to be damaged. The integration parts of the PID controller use the sensor values x_{seB} and y_{seB} for the feedback.

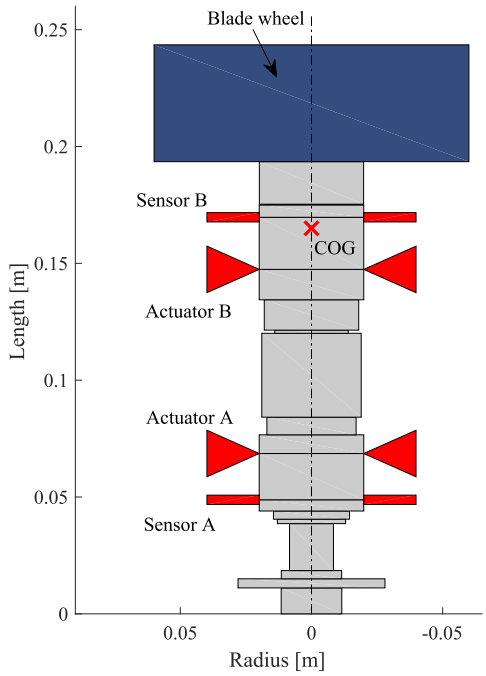

Fig. 9. Geometry of the stabilized rotor.

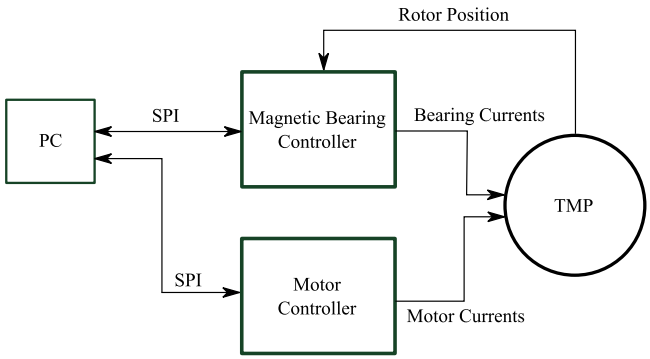

Fig. 10. Experimental setup.

For the optimization process for the controller design, the following parameters are used:

$$\mathbf{Q} = \mathrm{diag}([1000\ 1000\ 1000\ 1000\ 1\ 1\ 1\ 1\ 0.001\ 0.001])$$
$$\mathbf{R} = \mathrm{diag}([0.1\ 0.1])\ r = 0.9998 \quad T_s = 100\,\mu\mathrm{s}. \tag{47}$$

A. Start Up of the Underactuated System

To evaluate the functionality of the proposed operation mode, the step response from a safety bearing contact to a stable levitation was measured (see Fig. 11). The TMP is mounted vertical and the gravitation force affects only the z-direction. The integration part of the controller defines the steady state of the system. Without an integration part, the steady state could also be a safety bearing contact, because of additional forces caused by an asymmetric behavior of the bearings. The reason why the position near the damaged actuator x_{seA} rises faster than

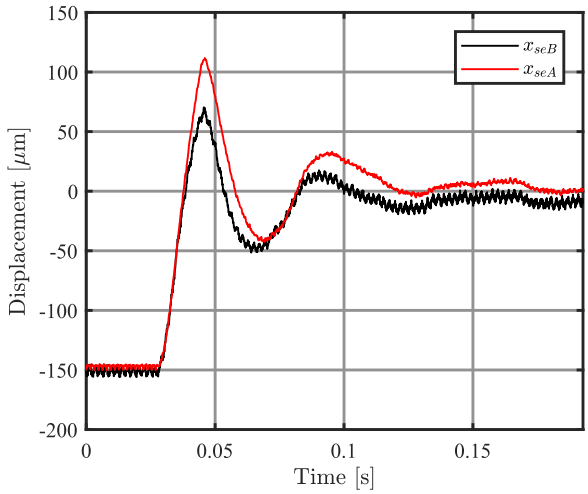

Fig. 11. Startup of an underactuated AMB system at standstill for the vertical case.

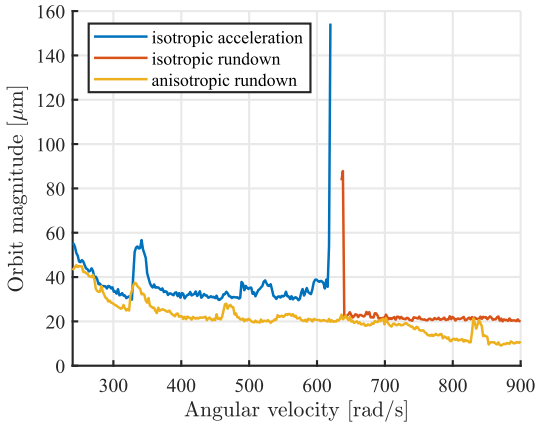

Fig. 12. Speed-dependent orbit of an isotropic and an anisotropic system with a defective actuator.

the position x_{seB} lies in the fact that the COG is not between the actuators.

B. Speed-Dependent Orbit of an Isotropic and an Anisotropic Actuator

To verify the stability dependence on the isotropy of the negative stiffness, the magnitude of the orbit of the controlled actuator was measured. Therefore, Fig. 12 shows the maximum orbit magnitude depending on the angular velocity of the rotor. In the isotropic case, the experiment was realized twice, because the system becomes unstable for a certain speed range. The first experiment was made from low speeds to the unstable region (isotropic acceleration) and the second from 900 rad/s down to the unstable region (isotropic rundown). For the anisotropic bearing one, rundown experiment is enough because of the stability in the operating range. The parameters of the isotropic bearing are listed in Table I. The isotropic magnetic bearing becomes unstable at an angular velocity of about 620 rad/s, which correlates with the result of (29). To generate the anisotropic behavior, the parameter k_{xB} was increased by 20 %. This was

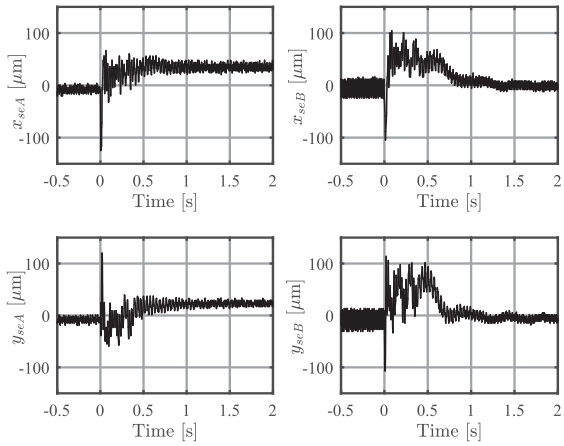

Fig. 13. Restabilization after a safety bearing contact at 5000 r/min. The safety bearing contact is caused by turning OFF the controller for a certain time.

done by an additional positive feedback, which is only used to affect the negative stiffness in a specific direction. As expected, in the anisotropic case, the system shows no unstable region in the explored angular velocity range. The lower orbit in the stable regions of the anisotropic bearing results from the higher negative stiffness and, thus, from a higher resulting stiffness of the LQR controlled system. The reason why the measurements were only realized down to 200 rad/s lies in a high resulting orbit caused by the unbalance vibration for low angular velocities.

C. Stabilization in the Case of a Damaged Actuator

With the proposed operation mode, it should be possible to stabilize the rotor in the case of a damaged actuator. To verify this functionality, Fig. 13 shows the behavior of the system after the deactivation of the controller for the actuator A. In this experiment, the system is fully actuated at the beginning. Afterward, the whole control structure was switched OFF for 10 ms to simulate the detection time of a damaged actuator. To stabilize the system again, the control structure is switched to the underactuated controller in the next step. Thus, Fig. 13 proves the stabilization in the case of an actuator error. The position at the defective actuator has a constant error in the vertical case. This error is caused by a not ideal symmetric behavior of the magnetic bearings. The high settling time of the positions at the controlled actuators lies on the low integration parts of the controller. In summary, it can be stated that the proposed operation mode can stabilize the rotor using linear controllers for a defective radial actuator.

VIII. Conclusion

In this article, an operation mode for AMB systems has been proposed for the case of an underactuation caused by a defective actuator. The underactuated operation mode uses the operating point, which is defined by the negative stiffness of the defective radial actuator and possible constant disturbance forces. The system is stabilized using LQ optimized PID controller. The calculation of the reachability matrix results in an angular

velocity where the system is not reachable. The not reachable poles are marginally stable, and therefore, the system is also marginally stable for a defined angular velocity. However, for a real system, the actuators are not ideally isotropic. By assuming an anisotropic behavior, the system becomes reachable. The proposed operation mode for magnetic bearings has been validated by experimental tests.

REFERENCES

[1] G. Schweitzer, *Magnetic Bearings: Theory, Design, and Applications to Rotating Machinery*. Berlin, Germany: Springer, 2009.

[2] H. Bleuler, "Decentralized control of magnetic rotor bearing systems," Ph.D. dissertation, ETH Zurich, Zürich, Switzerland, 1984.

[3] E. Tang, B. Han, and Y. Zhang, "Optimum compensator design for the flexible rotor in magnetically suspended motor to pass the first bending critical speed," *IEEE Trans. Ind. Electron.*, vol. 63, no. 1, pp. 343–354, Jan. 2016.

[4] X. Zhou, J. Fang, and S. Xu, "Analysis and suppression of the suspended rotor displacement fluctuation influence for motor system," *IEEE Trans. Ind. Electron.*, vol. 61, no. 12, pp. 6966–6974, Dec. 2014.

[5] C. Zhang and K. J. Tseng, "Design and FEM analysis of a flywheel energy storage system assisted by integrated magnetic bearings," in *Proc. 30th Annu. Conf. Ind. Electron. Soc.*, May 2004, pp. 1634–1639.

[6] S.-M. Yang, "Electromagnetic actuator implementation and control for resonance vibration reduction in miniature magnetically levitated rotating machines," *IEEE Trans. Ind. Electron.*, vol. 58, no. 2, pp. 611–617, Feb. 2011.

[7] W. Tong and F. Jiancheng, "A feedback linearization control for the nonlinear 5-DOF flywheel suspended by the permanent magnet biased hybrid magnetic bearings," *Acta Astronautica*, vol. 79, pp. 131–139, Oct. 2012.

[8] D. Wimmer, M. Hutterer, M. Hofer, and M. Schrdl, "Space vector modulation strategies for self-sensing three-phase radial active magnetic bearings," *Actuators*, vol. 8, no. 2, May 2019.

[9] T. Nenning, M. Hofer, M. Hutterer, and M. Schrödl, "Setup with two self-sensing magnetic bearings using differential 3-active INFORM," in *Proc. Int. Symp. Magn. Bearings*, Aug. 2014, pp. 689–692.

[10] M. Hutterer, M. Hofer, T. Nenning, and M. Schrödl, "LQG control of an active magnetic bearing with a special method to consider the gyroscopic effect," in *Proc. Int. Symp. Magn. Bearings*, Aug. 2014, pp. 54–59.

[11] M. Hutterer, M. Hofer, and M. Schrödl, "Decoupled control of an active magnetic bearing system with a high gyroscopic rotor," in *Proc. IEEE Int. Conf. Mechatronics*, Mar. 2015, pp. 210–215.

[12] M. Cole and W. Fakkaew, "An active magnetic bearing for thin-walled rotors: Vibrational dynamics and stabilizing control," *IEEE/ASME Trans. Mechatronics*, vol. 23, no. 6, pp. 2859–2869, Dec. 2018.

[13] Y. N. Zhuravlyov, "On LQ-control of magnetic bearing," *IEEE Trans. Control Syst. Technol.*, vol. 8, no. 2, pp. 344–350, Mar. 2000.

[14] S. E. Mushi, Z. Lin, and P. E. Allaire, "Design, construction, and modeling of a flexible rotor active magnetic bearing test rig," *IEEE/ASME Trans. Mechatronics*, vol. 17, no. 6, pp. 1170–1182, Dec. 2012.

[15] S. Zheng, B. Han, Y. Wang, and J. Zhou, "Optimization of damping compensation for a flexible rotor system with active magnetic bearing considering gyroscopic effect," *IEEE/ASME Trans. Mechatronics*, vol. 20, no. 3, pp. 1130–1137, Jun. 2015.

[16] T. Baumgartner and J. W. Kolar, "Multivariable state feedback control of a 500 000-r/min self-bearing permanent-magnet motor," *IEEE/ASME Trans. Mechatronics*, vol. 20, no. 3, pp. 1149–1159, Jun. 2015.

[17] K.-Z. Liu and R. He, "A nonlinear output feedback control method for magnetic bearing systems," in *Proc. Eur. Control Conf.*, 2003, pp. 3401–3406.

[18] S.-S. Yu, S.-J. Wu, and T.-T. Lee, "Application of neural-fuzzy modeling and optimal fuzzy controller for nonlinear magnetic bearing systems," in *Proc. IEEE/ASME Int. Conf. Adv. Intell. Mechatronics*, Jul. 2003, pp. 7–11.

[19] C. Liu, G. Liu, and J. Fang, "Feedback linearization and extended state observer-based control for rotor-AMBs system with mismatched uncertainties," *IEEE Trans. Ind. Electron.*, vol. 64, no. 2, pp. 1313–1322, Feb. 2017.

[20] K. Zheng, H. Liu, and L. Yu, "Robust fuzzy control of a nonlinear magnetic bearing system with computing time delay," in *Proc. IEEE/ASME Int. Conf. Adv. Intell. Mechatronics*, Jul. 2008, pp. 839–843.

[21] H. S. Zad, T. I. Khan, and I. Lazoglu, "Design and adaptive sliding-mode control of hybrid magnetic bearings," *IEEE Trans. Ind. Electron.*, vol. 65, no. 3, pp. 2537–2547, Mar. 2018.

[22] D. Pucci, F. Romano, and F. Nori, "Collocated adaptive control of underactuated mechanical systems," *IEEE Trans. Robot.*, vol. 31, no. 6, pp. 1527–1536, Dec. 2015.

[23] R. Olfati-Saber, "Nonlinear control of underactuated mechanical systems with application to robotics and aerospace vehicles," Ph.D. dissertation, Dept. Elect. Eng. Comput. Sci., Massachusetts Inst. Technol., Cambridge, MA, USA, 2001.

[24] X. Lai, Y. Wang, M. Wu, and W. Cao, "Stable control strategy for planar three-link underactuated mechanical system," *IEEE/ASME Trans. Mechatronics*, vol. 21, no. 3, pp. 1345–1356, Jun. 2016.

[25] P. Oryschuk, A. Salerno, A. M. Al-Husseini, and J. Angeles, "Experimental validation of an underactuated two-wheeled mobile robot," *IEEE/ASME Trans. Mechatronics*, vol. 14, no. 2, pp. 252–257, Apr. 2009.

[26] S. Kim and S. Kwon, "Nonlinear optimal control design for underactuated two-wheeled inverted pendulum mobile platform," *IEEE/ASME Trans. Mechatronics*, vol. 22, no. 6, pp. 2803–2808, Dec. 2017.

[27] N. Muskinja and B. Tovornik, "Swinging up and stabilization of a real inverted pendulum," *IEEE/ASME Trans. Ind. Electron.*, vol. 53, no. 2, pp. 631–639, Apr. 2006.

[28] A. Schulz, M. Schneeberger, and J. Wassermann, "A reliability analysis of switching amplifier concepts for active magnetic bearings," in *Proc. IEEE Int. Conf. Ind. Technol.*, Dec. 2006, pp. 1460–1465.

[29] M. Li, B. Palazzolo, A. Kenny, A. Provenza, R. Beach, and A. Kascak, "Fault-tolerant homopolar magnetic bearings," *IEEE Trans. Magn.*, vol. 40, no. 5, pp. 3308–3318, Sep. 2004.

[30] E. Maslen and D. Meeker, "Fault tolerance of magnetic bearings by generalized bias current linearization," *IEEE Trans. Magn.*, vol. 31, no. 3, pp. 2304–2314, May 1995.

[31] M. Noh, S. Cho, J. Kyung, S. Ro, and J. Park, "Design and implementation of a fault-tolerant magnetic bearing system for turbo-molecular vacuum pump," *IEEE Trans. Mechatronics*, vol. 10, no. 6, pp. 626–631, Dec. 2005.

[32] R. Tedrake, "Underactuated robotics: Learning, planning, and control for efficient and agile machines," Course Notes for MIT 6.832, Massachusetts Inst. Technol., Cambridge, MA, USA, 2009.

[33] J. Schmied and A. Kosenkov, "Practical controller design for rotors on magnetic bearings by means of an efficient simulation tool," in *Proc. ASME Turbo Expo*, Jun. 2013.

[34] R. Herzog, P. Bühler, C. Gähler, and R. Larsonneur, "Unbalance compensation using generalized notch filters in the multivariable feedback of magnetic bearings," *IEEE Trans. Control Syst. Technol.*, vol. 4, no. 5, pp. 580–586, Sep. 1996.

[35] M. Friswell, J. Penny, S. Garvey, and A. Lees, *Dynamics of Rotating Machines*. Cambridge, U.K.: Cambridge Univ. Press, 2010.

[36] M. Ahrens, L. Kucera, and R. Larsonneur, "Performance of a magnetically suspended flywheel energy storage device," *IEEE Trans. Control Syst. Technol.*, vol. 4, no. 5, pp. 494–502, Sep. 1996.

[37] M. Schredl, "Sensorless control of AC machines at low speed and standstill based on the 'INFORM' method," in *Proc. Conf. Rec. IEEE Ind. Appl. Conf. 31st IAS Annu. Meeting*, Oct. 1996, pp. 270–277.

Markus Hutterer (Member, IEEE) was born in Austria in 1989. He received the B.Sc. degree in mechatronics from the University of Applied Sciences Wiener Neustadt, Wiener Neustadt, Austria, in 2012, and the Dipl.Ing. and doctoral degrees from Vienna University of Technology, Vienna, Austria, in 2014 and 2018, respectively, both in electrical engineering.

He is currently a Postdoctoral Researcher with the Institute of Energy Systems and Electrical Drives, Vienna University of Technology. His main research interests include modeling of dynamic systems, controller design for magnetic bearing applications for rotating machinery, design of magnetic bearings, and self-sensing techniques for electromechanical drives and actuators.

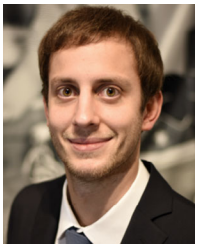

Dominik Wimmer was born in Austria in 1991. He received the B.Sc. degree in electrical engineering and the Dipl.Ing. degree in energy systems and automation technology from the Vienna University of Technology (TU Wien), Vienna, Austria, in 2015 and 2017, respectively.

Since 2017, he has been with the Institute of Energy Systems and Electrical Drives, TU Wien. His research interest includes magnetic bearings, including the appropriate power electronics, AMB design, digital controller design, and system identification in context of self-sensing control.

Manfred Schrödl (Member, IEEE) was born in Austria in 1958. He received the Dipl.Ing., doctoral, and habilitation degrees from the Vienna University of Technology, Vienna, Austria, in 1982, 1987, and 1992, respectively, all in electrical engineering.

Between 1992 and 1996, he was the Head of the Development Department, ELIN Traction, Vienna, Austria. Between 1996 and 1998, he was the Head of the Central Technical Division, Austria Antriebstechnik Bauknecht AG, Spielberg, Austria. Since 1998, he has been a Full Professor of electrical drives and machines with the Vienna University of Technology, where he is also the Head of the Institute of Energy Systems and Electrical Drives. He has authored more than 100 publications and holds several patents, mainly in the fields of sensorless control of ac machines (e.g., the INFORM method) and special motors. His main research fields include sensorless-controlled ac machines, high-speed drives, and electrical drives for automotive applications.